**Al-Nahrain J. Eng. Sci. 29(2) 371-383, 2026**
**Original Article**

# Robust, Policy-Tunable Optimization of Diesel Plastic Fuel/α-Terpineol Blends Across the Duty Map

**Satyasaibaba Pitta[1], Bharath Raju Lodd Battu[2], Mallikarjunachari Gangapuram[3], Sai Srikanth Vemuri[4]*, Prabhu Kishore Nutakki[5] and Prasad Kumar Putha [6]●.**

*1Department of Mechanical Engineering, University College of Engineering, JNTUK, Kakinada-533003, Andhra Pradesh, India.*
*2Department of Mechanical Engineering, Malla Reddy Technical Campus (A Constituent Unit of Malla Reddy Vishwavidyapeeth, Deemed to be University), Hyderabad-500014, India.*
*3Department of Mechanical Engineering, PACE Institute of Technology and Sciences (A), Ongole-523272, India.*
*4Department of Mechanical Engineering, Mallareddy College of Engineering and Technology, Maisammaguda Village, Kompally, Secunderabad-500100, Telangana, India.*
*5Department of Mechanical Engineering, MLR Institute of Technology, Hyderabad-500043, India.*
*6Department of Mechanical Engineering, VNR Vignana Jyothi Institute of Engineering and Technology, Hyderabad-500090, India.*

●*These authors contributed equally to this work*

**DOI:** https://www.doi.org/10.29194/NJES.29020371

**Received:** Nov. 5, 2025 **Revised:** Jan. 17, 2026 **Accepted:** Feb. 26, 2026 **Published:** June 20, 2026

## Abstract

This study establishes a risk aware, multi objective methodology to select diesel plastic fuel α-terpineol blends that deliver robust engine performance across operating loads in a common rail direct injection diesel engine. Heterogeneous responses brake thermal efficiency, brake specific fuel consumption, oxides of nitrogen, carbon monoxide, hydrocarbons, smoke, and exhaust gas temperature are mapped to a unitless desirability scale and aggregated by load. Conditional Value at Risk across loads then prioritizes worst case behavior. By Conditional Value at Risk at level 0.20, the ranking is: diesel 0.242, diesel plastic fuel with 15% α-terpineol 0.197, 10% α-terpineol is 0.177, 5% α-terpineol is 0.157, diesel plastic fuel is 0.141, waste plastic fuel is 0.081. Relative to neat diesel plastic fuel, worst-case performance improves by 11% at 5% α-terpineol, 26% at 10% α-terpineol, and 40% at 15% α-terpineol, with the 100% load consistently governing the tail. Average brake specific fuel consumption decreases from 0.4553 to 0.4217 kg/kWh at 15% α-terpineol, average exhaust gas temperature falls from 321.4 to 293.0°C. Duty map mean oxides of nitrogen reduce from 512 to 474 ppm, hydrocarbons fall from 42.67 to 35.73 ppm. At full load, carbon monoxide declines from 0.52 to 0.46 %vol., and smoke opacity decreases from 52.28 to 49.71%. Within the tested window, 15% α-terpineol in diesel plastic fuel is the risk aware first choice, with 10% α-terpineol a near optimal alternative. The methodology remains stable under risk aversion and weighting changes at high-load calibration.

**Keywords:** *Diesel Plastic Fuel, A-Terpineol, Conditional Value at Risk, Quantile Based Desirability Functions, Worst Case Performance, Engine Calibration Robustness.*

**Corresponding author:** Provide the corresponding author information and publisher here. E-mail address: satyasaibabapitta@gmail.com

## 1. Introduction

Waste plastic pyrolysis routes yield Diesel plastic fuel (DPF) streams with attractive heating values but oxygen deficiency, variable cetane quality, and heavier aromatics that lengthen ignition delays and aggravate smoke/hydrocarbon (HC) at high load in diesel engines [1]. Alcoholic oxygenates can counter these deficits by supplying in fuel oxygen and improving mixture preparation, yet they also shift the Oxides of nitrogen (NOx) particulate matter and Brake thermal efficiency (BTE), Brake specific fuel consumption (BSFC) balance in a load dependent manner. The field lacks a principled, risk aware blend selection procedure that optimizes efficiency and multipollutant outcomes across the duty map rather than at a single operating point. Recent DPF engine studies and property assessments underline both the promise and the variability of outcomes with plastic oil blends, motivating a structured optimization that guards against worst case operating conditions [2, 3].

Binary and ternary diesel blends with higher alcohol consistently show smoke/carbon monoxide (CO) reductions and condition dependent efficiency changes. For instance, systematic testing of n-pentanol diesel blends over multiple loads and speeds maps clear trade-offs and demonstrates that benefits intensify at higher load/speed windows [4, 5]. DPF blends with ethanol or pentanol likewise report improved BTE and smoke with tuning, though NOx and ignition delay responses remain sensitive to load and injection strategy [6]. In parallel, terpene family oxygenates are gaining attention where thermophysical data and recent combustion and flame speciation indicate favorable mixing behavior, high energy density, and soot pathway differences [7, 8].

Although alternative fuels for diesel engines are now well established, their practical adoption is ultimately constrained by decision complexity rather than by fuel availability alone. The same blend can simultaneously improve smoke and CO while penalizing NOx, ignition delay, or efficiency, and these responses vary nonlinearly with both operating controls and blend composition. In this regard, best fuel blend is not a property of the blend in isolation, it is an optimization outcome under explicit priorities and constraints. Consequently, optimization methods are not peripheral add-ons but the mechanism by which alternative fuels become deployable. They demonstrate Pareto trade-offs, encode regulatory or fleet preferences, and prevent calibration decisions that look acceptable on average yet fail at worst case duty regions. This need is amplified for waste derived fuels whose performance dispersion across loads is often wider, making robustness across the duty map a first-order requirement rather than a refinement.

Multi-objective optimization has become central to tune diesel engine operating on alternative fuels because performance (BTE/BSFC) and regulated emissions (NOx, smoke, CO/HC) respond nonlinearly to both operating parameters and blend composition [9, 10]. Studies therefore cast calibration and blend selection as a multi-criteria decision problem, either seeking Pareto trade-offs or constructing single index optima aligned with policy or fleet priorities [11, 12]. Response Surface Methodology (RSM) coupled with desirability functions remains widely used to model coupled responses and identify compromise set points with modest experimental cost. Hybrid strategies and data driven surrogates extend optimization to larger design spaces, multiple operating conditions, and composition control interactions that are difficult to resolve experimentally [13, 14]. Recent study also emphasized moving beyond mean targets toward robustness to guard against high load outliers and constraint violations that often dominate real world acceptability [15]. In this context, optimization is not merely a post-processing step, it is the mechanism that translates alternative fuel potential into deployable decisions by making trade-offs explicit, enforcing constraints, and revealing whether gains persist under realistic operating variability.

Despite encouraging performance and smoke reductions reported for diesel-plastic and alcohol co-blends, many studies demonstrate optimality at a single operating point or under average aggregation, even though alternative fuels exhibit heterogeneous responses across the duty map. This leaves worst-case regions insufficiently controlled, even when averages look acceptable, and encourages decisions that may appear favorable in a narrow window yet become non-compliant under high load operation. Moreover, heterogeneous engine responses are often normalized with ad-hoc scaling or combined via mean indices, which can obscure tail behavior and policy trade-offs. Higher alcohol and DPF blends can deliver cleaner premixed burning and improved BTE, their benefits remain dependent on load and sensitive to injection/ EGR settings. This highlights the need for a methodology that explicitly aggregates outcomes across operating scenarios and guards against adverse tails. Terpene family oxygenates show promising thermophysical and soot pathway attributes, yet engine scale evaluation in DPF blends remains limited, reinforcing both a mechanistic and an optimization gap for this class.

Accordingly, this study introduces a scenario-based, risk-aware multi-objective methodology for DPF alcohol blend selection across the duty map of a CRDi diesel engine. Heterogeneous engine metrics are mapped to quantile calibrated sigmoid desirability and aggregated per load using a geometric mean, then aggregated across loads using Conditional Value-at-Risk (CVaR) to explicitly control worst case behavior. Unlike mean desirability/ RSM formulations, this method enables configurable objective needs (policy, economy, and robustness) together with soft constraints on EGT, yielding transparent, tail robust decisions for alternative fuel deployment.

This study aims to establish a principled, risk aware multi objective methodology for selecting and calibrating DPF alcohol blends in a CRDi diesel engine. Specifically, it maps heterogeneous engine responses BTE, BSFC, NOx, CO, smoke, and EGT into quantile calibrated sigmoid desirability. Assess aggregates performance and emissions across loads using CVaR to prioritize worst case behavior. Demonstrate configurable objective flavors (policy lean with stronger NOx weighting, economy lean emphasizing BTE/BSFC, and robustness lean with soft penalties on excessive EGT). Validate the recommended blend(s) against baselines through comparative analyses over representative loads, with an optional physics aware surrogate for continuous search between tested blend levels.

## 2. Materials and Methods

### 2.1 Fuels, additive, and blend preparation

Four base fuels were evaluated such as commercial diesel, Waste plastic oil/fuel (WPF), produced from waste plastic pyrolysis process, Diesel plastic fuel (DPF=50 vol.% diesel + 50 vol.% WPF), and DPF blended with the selected alcoholic oxygenate (α-terpineol) at 5, 10, and 15 vol.% (DPF-αT05/10/15). Blends were prepared gravimetrically at ambient laboratory conditions (22-25°C) using amber glassware, magnetically stirred (≥15 min) and left to stand (≥24 h) to screen for phase separation. All test fuels passed visual miscibility checks. Before engine testing, each blend was micro filtered (5 μm PTFE) and stored in sealed, airtight containers. Key properties were measured following standard procedures, as shown in Table 1, density 15°C (ASTM D4052), kinematic viscosity 40°C (ASTM D445), flash point (ASTM D93), elemental C/H/N/O (ASTM D5291/D5622), and higher heating value by bomb calorimetry (ASTM D240). WPF is included as an upstream baseline/ reference (alongside diesel) to report the intrinsic physicochemical characteristics of the plastic derived oil and to demonstrate how blending with diesel to form DPF shifts these properties toward engine compatibility.

**Table 1.** The properties of base fuel types and their blends

| Property | WPF | Diesel | DPF | DPF-αT05 | DPF-αT10 | DPF-αT15 |
|---|---|---|---|---|---|---|
| Kinematic viscosity cST @40$^0$C | 3.64 | 2.12 | 2.88 | 2.78 | 2.75 | 2.71 |
| Density (kg/m$^3$) | 845 | 840 | 842.5 | 841.1 | 841.3 | 841.7 |
| Flash point ($^0$C) | 62 | 54 | 58 | 59.7 | 61.3 | 63 |
| Calorific value (kJ/kg) | 42900 | 46500 | 44700 | 44520 | 44342 | 44165 |
| Cetane index | 38 | 54.5 | 44 | 43.35 | 42.7 | 42.05 |

| | | | | | | |
|---|---|---|---|---|---|---|
| Self-ignition temperature ($^0$C) | 258 | 210 | 242 | 244.3 | 246.1 | 247.8 |
| Carbon content (wt.%) | 780.3 | 85 | 82 | 81.77 | 81.55 | 81.32 |
| Hydrogen content (wt.%) | 12 | 13 | 12 | 11.99 | 11.97 | 11.96 |
| Nitrogen content (wt.%) | 1.29 | 0 | 0.91 | 0.86 | 0.81 | 0.76 |
| Oxygen content (wt.%) | 0 | 0 | 0 | 0.57 | 1.14 | 1.7 |

## 2.2 Engine test bench and instrumentation

The present experiments were carried out on a Kirloskar TV1, single cylinder CRDi diesel engine. The engine was operated at a constant speed of 1500 rpm with the rail pressure maintained at 600 bar, delivering a rated output of 3.5 kW. The electronic control unit was interfaced with the in-cylinder pressure sensing system, and load was applied using an eddy current dynamometer. Temperatures were monitored using K-type thermocouples installed at the air intake, fuel line, cooling circuit, and exhaust stream. The engine technical specifications are summarized in Table 2. A series of steady state tests was conducted at 20%, 40%, 60%, 80%, and 100% load using Diesel, WPF, DPF, DPF-αT05, DPF-αT10, and DPF-αT15 as test fuels. Baseline measurements were first established with neat diesel. Engine performance was quantified through BTE and BSFC computed from the measured torque, speed, and fuel flow data. Regulated exhaust emissions (NOx, $CO_2$, CO, and HC) were measured using a five-gas analyzer (AVL DiGas 444N), and smoke opacity was recorded with an AVL 437C smoke meter. All signals were logged through a data acquisition unit and recorded on a computer running Engine Soft. For each operating condition, the engine was allowed to run for approximately 15 min to reach thermal equilibrium, followed by an additional 10-15 min stabilization prior to data capture. Each test point was repeated three times, and the reported values represent the mean of the repeat measurements. A schematic of the experimental arrangement is provided in Fig. 1, while the measurement range, resolution, and stated accuracy of the instruments are listed in Table 3.

**Table 2.** The specifications of CRDi engine and eddy current dynamometer

| Parameter | Remarks |
|---|---|
| Stroke (mm) | 110 |
| Bore (mm) | 87.5 |
| No. of cylinders | 1 |
| Rated speed (rpm) | 1500 |
| Swept volume (cc) | 661 |
| Rated power @1500 rpm (kW) | 3.5 |
| Fuel injection pressure (bar) | 600 |
| Fuel injection timing ($^0$CA) bTDC | 23 |
| Engine cooling | Water |
| Dynamometer capacity (kW) | 7.46 |
| Speed range (rpm) | 1500-5000 |
| Strain gauge load cell (kg) | 0-50 |

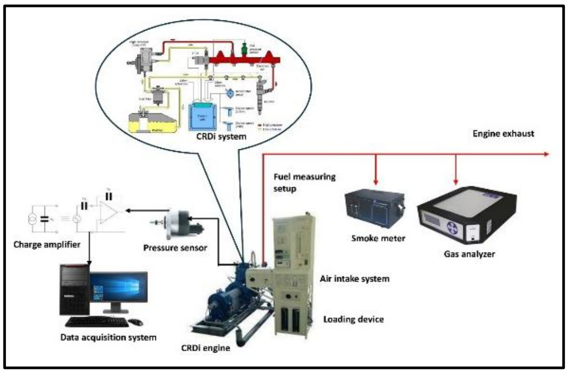


**Figure 1.** The schematic of the experimental Setup

**Table 3.** The measuring range, accuracy and resolution of the instruments used

| Measured quantity | Range | Resolution | Accuracy |
|---|---|---|---|
| CO2 | 0-20% | ± 0.1% | ±0.03% |
| CO | 0-9.99% | 0.01% | ±0.02% |
| NOx | 0-5000 ppm | 1 ppm | ±5 ppm |
| HC | 0-20000 ppm | 1 ppm | ±10 ppm |
| Speed | 0-2000 rpm | 5 rpm | ±10 rpm |
| Smoke opacity | 0-100% | 0.10% | ±1% |
| EGT | 0-1000 $^0$C | ±1 $^0$C | ±1 $^0$C |

## 2.3 Operating conditions and test matrix

Tests were performed at constant engine speed (rated speed 1500±5 rpm) across five brake load setpoints 20, 40, 60, 80, and 100% of rated load. For each fuel, the engine stabilized at each setpoint until coolant, oil, and EGT drifted <±2% over a 2 min window. Data were then logged for ≥120 s. The order of fuels and loads was randomized to mitigate drift and carry over. A purge run (diesel) was used between fuels. All conditions were repeated thrice and averaged. The mixture strength was quantified for each fuel-load point using the excess air ratio (λ) and the corresponding equivalence ratio (ϕ), summarized in Table 4. Across all fuels, λ decreased monotonically with load, and the between fuel differences at a fixed load were modest relative to the load shift, supporting that the observed performance and emission trends predominantly reflect fuel effects rather than systematic lean-rich bias.

**Table 4.** Mixture strength (λ and ϕ) across the operating matrix

| Load (%) | Diesel - λ (ϕ) | WPF - λ (ϕ) | DPF - λ (ϕ) | DPF-αT05 - λ (ϕ) | DPF-αT10 - λ (ϕ) | DPF-αT15 - λ (ϕ) |
|---|---|---|---|---|---|---|
| 20 | 4.640 (0.216) | 4.874 (0.205) | 4.755 (0.210) | 4.876 (0.205) | 4.969 (0.201) | 5.082 (0.197) |
| 40 | 3.282 (0.305) | 3.067 (0.326) | 3.187 (0.314) | 3.268 (0.306) | 3.384 (0.296) | 3.517 (0.284) |
| 60 | 2.806 (0.356) | 2.425 (0.412) | 2.611 (0.383) | 2.677 (0.374) | 2.772 (0.361) | 2.881 (0.347) |
| 80 | 2.466 (0.406) | 1.957 (0.511) | 2.186 (0.457) | 2.242 (0.446) | 2.321 (0.431) | 2.412 (0.415) |
| 100 | 2.060 (0.485) | 1.606 (0.623) | 1.807 (0.553) | 1.853 (0.540) | 1.919 (0.521) | 1.994 (0.501) |
| Range | 2.060-4.640 | 1.606-4.874 | 1.807-4.755 | 1.853-4.876 | 1.919-4.969 | 1.994-5.082 |

## 2.4 Uncertainty analysis and statistical confidence

To quantify the reliability of the engine responses, an uncertainty analysis was performed for the principal outputs, namely BTE, BSFC, NOx, HC, CO, CO2, smoke opacity, and EGT. For a generic measured quantity y obtained from repeated measurements, the Type-A standard uncertainty was evaluated from the sample standard deviation s_y over n repeats as shown in equation (1).

$$u_A(y) = \frac{s_y}{\sqrt{n}}, s_y = \sqrt{\frac{1}{n-1}\sum_{i=1}^{n}(y_i - \bar{y})^2}, \bar{y} = \frac{1}{n}\sum_{i=1}^{n} y_i \quad \ldots(1)$$

The Type-B standard uncertainty u_B (y) was obtained from the stated instrument accuracy, the standard uncertainty is shown in equation (2).

$$u_B(y) = \frac{B}{\sqrt{3}} \quad \ldots(2)$$

The combined standard uncertainty is then computed using the root sum-of-squares combination, as shown in equation (3).

$$u_C(y) = \sqrt{u_A(y)^2 + u_B(y)^2} \quad \ldots(3)$$

In the present study, the overall uncertainty is ±3.21%.

## 2.4 Multi objective optimization methodology

In this study, the optimization problem has been implemented as a blend selection decision over the fuel blend set X, where the decision variable $xx$ denotes a specific DPF-α terpineol blend level. The objective is to identify the blend that delivers the most favorable multi-criteria compromise between efficiency and fuel economy (BTE, BSFC) and regulated emissions (NOx, smoke, CO, HC, CO2), not at a single operating point, but across the duty map. To make heterogeneous engine responses comparable and aggregation defensible, each measured metric at each load is first transformed into a unitless desirability score d_j (x,l) ∈ (0,1) using a calibrated quantile sigmoid mapping. This desirability is then combined at a given load using a weighted geometric mean, where exponent weights ϱ_j encode the relative importance of criteria. Finally, the per load composite scores are aggregated across loads using Conditional Value-at-Risk 〖CVaR〗_α, so that the selected blend maximizes performance in the worst-load tail, rather than optimizing only the mean.

### 2.4.1 Notation and data structure

Let $x \in X$ denote the blend level (discrete set of tested blends, or a continuous interval $[x_{min}, x_{max}]$

$l \in L = \{l_1, \ldots, l_L\}$ index engine loads

j∈ $J$ index response metrics

$$J \in \{BTE, BSFC, NOx, CO, Smoke, EGT, ID\}$$

$y_j(x, l)$ be the steady state mean of metric $j$ at $(x, l)$

Partition $J$ into maximize set $J^+ = \{BTE\}$, minimize set $J^- = J \backslash J^+$

### 2.4.2 Quantile calibrated sigmoid desirability

To remove unit/scale effects and avoid arbitrary min-max bounds, each metric is mapped into a unitless score $d_j \in (0,1)$ using the empirical distribution of that metric over all observed $(x, l)$.

Compute quantiles ($q_{0.2}$, $q_{0.5}$, $q_{0.8}$) from $\{y_j(x, l)\}_{x,l}$. Define a slope,

$$k_j = \frac{2 ln3}{q_{0.8,j} - q_{0.2,j}} \quad (q_{0.2} \mapsto 0.25 \text{ and } q_{0.8} \mapsto 0.75) \quad \ldots(4)$$

For maximizing metrics ($J \in J^+, e.g., BTE$),

$$d_j(y) = \sigma\left(k_j(y - q_{0.5,j})\right) = \left(1 + exp[-k_j(y - q_{0.5,j})]\right)^{-1} \quad \ldots(5)$$

For minimizing metrics

($J \in J^-, e.g., NOx, Smoke, BSFC, CO, EGT, ID$),

$$d_j(y) = \sigma\left(-k_j(y - q_{0.5,j})\right) = \left(1 + exp[+k_j(y - q_{0.5,j})]\right)^{-1} \quad \ldots(6)$$

To reflect policy priorities, each metric received an exponent $\rho_j$ (e.g., $\rho_{NOx}, \rho_{smone} \geq 1$) and the per load aggregate desirability,

$$\bar{d}_j(y) = \left(d_j(y)\right)^{\rho_j} \quad \ldots(7)$$

$\rho_j > 1$ sharpens the penalty for underperformance, $\rho_j < 1$ softens it. Because $d_j \in (0,1)$, exponentiation preserves order.

### 2.4.3 Per load aggregation across metrics

At each load ℓ, combine metric level desirability by the geometric mean (multiplicative compromise),

$$D_{geo}(x, l) = exp\left(\frac{1}{|J|}\sum_{j \in J} ln\bar{d}_j(y_j(x, l))\right) \quad \ldots(8)$$

This yields one load specific score per $(x, l)$, with $D_{geo} \in (0,1)$

### 2.4.4 Risk aggregation across loads

Treat loads as scenarios for operating variability. For any blend $x$, collect $\{D_{geo}(x, l) : l \in L\}$

Let $D_1 \leq D_2 \leq \cdots \leq D_L$ be the order statistics of these $L$ values.

Value-at-Risk (VaR) at level $\alpha \in (0,1]$,

$$VaR_\alpha(x) = D_k, k = \lceil \alpha L \rceil \quad \ldots(9)$$

Conditional Value-at-Risk (CVaR) a.k.a. expected shortfall,

$$CVaR_\alpha(x) = \frac{1}{k}\sum_{r=1}^{k} D_{(r)} \text{ with } k = \lceil \alpha L \rceil \quad \ldots(10)$$

This emphasizes the worst α-fraction of loads. Typical choices: α=0.2 (baseline), α=0.3 (policy-lean)

### 2.4.5 Soft constraints

Constraints on stability/safety (e.g., $ID > \tau_{ID}, EGT > \tau_{EGT}$) are integrated at the per load level via penalties on $D_{geo}$.

Binary (hard) penalty:

$$\hat{D}_{geo}(x, l) = \begin{cases} \gamma D_{geo}(x, l), if\ any\ c \in C\ violated\ at\ (x, l), \\ D_{geo}(x, l), otherwise, \end{cases} \quad \ldots(11)$$

With $\gamma \in (0,1)$ (e.g., $\gamma = 0.8$) and constraint set $C$ (ID, EGT, etc.,)

Smooth logistic penalty:

For a metric $m$ with upper threshold $\tau_m$,

$$p_m(y_m(x, l)) = \frac{1}{1 + exp\{k_m[y_m(x,l) - \tau_m]\}}, k_m > 0 \quad \ldots(12)$$

and overall penalty,

$$P(x, l) = \prod_{m \in C} p_m(y_m(x, l)) \quad \ldots(13)$$

Then use $\hat{D}_{geo}(x, l) = P(x, l) D_{geo}(x, l) \quad \ldots(14)$

Replace $D_{geo}$ by $\hat{D}_{geo}$ in the ordering for CVaR.

### 2.4.6 Objective flavors (policy, economy, robustness)

Policy lean: increase $\rho_{NOx}$ (and optionally $\rho_{smoke}$); use larger α (e.g., 0.3).

Economy lean: increase $\rho_{BTE}, \rho_{BSFC}$; keep α=0.2.

Robustness lean: keep α=0.2 and activate penalties $P(x, l)$.

These levers explicitly change how worst case loads shape the optimum.

### 2.4.7 Optimization problems

(A) Discrete optimization

With a finite set $X = \{x_1, \ldots, x_M\}$,

$$x^* \in argmax_{x \in X} CVaR_\alpha(x)$$

(B) Continuous extension

If a surrogate $\hat{y}_j(x,l)$ is trained (e.g., shape constrained spline/GP), define $\hat{d}_j$, $\widehat{D}_{geo}$, and $\widehat{CVaR}_\alpha(x)$ analogously, and solve $\max_{x\in[x_{min},x_{max}]} \widehat{CVaR}_\alpha(x)$ by grid search or gradient free methods.

### 2.4.8 Pareto and knee-point selection

Let $m(x)$ collect the expected metric values (or desirability) at a representative load (or averaged on load). With ideal (utopia) point $z^{ut}$ and nadir $z^{na}$, define normalized distances

$$\partial_{ut}(x) = \|[m(x) - z^{ut}] \oslash [z^{na} - z^{ut}]\|_2 \quad \ldots(15)$$

$$\partial_{na}(x) = \|[m(x) - z^{na}] \oslash [z^{na} - z^{ut}]\|_2 \quad \ldots(16)$$

and a knee score,

$$k(x) = \frac{\partial_{na}(x)}{\partial_{ut}(x)} \times CVaR_\alpha(x) \quad \ldots(17)$$

### 2.4.9 Uncertainty and significance

Bootstrap CVaR: For fixed $x$, resample loads with replacement $B$ times, recompute $CVaR_\alpha^{(b)}(x)$, and form percentile CIs,

$$CI_{0.95}(x) = \left[Q_{0.025}\left\{CVaR_\alpha^{(b)}(x)\right\}, Q_{0.975}\left\{CVaR_\alpha^{(b)}(x)\right\}\right]$$
…(18)

Ranking stability: Report the fraction of bootstrap replicates in which $x^*$ remains the top rank (or within $\Delta$ of the top) and include α-sweep and weight sweep plots to visualize sensitivity.

Practical defaults: α=0.2, $\rho_{NOx} = \rho_{smoke} = 1.3$, $\rho_{BTE} = 1.1$, $\rho_{BSFC} = \rho_{CO} = \rho_{EGT} = 1.0$, $\varepsilon = 10^{-12}$, $\gamma = 0.8$, $k_{EGT} \in [0.5,2.0]$

The methodology converts heterogeneous engine responses into comparable, policy tunable desirability, aggregates them per load with a multiplicative compromise, and then performs risk averse selection via CVaR across loads. The result is an optimal blend that is strong where it matters, most under the worst operating segments, while remaining transparent and reproducible. A numerical example is provided in the Appendix for DPF–αT15 at 100% load.

## 3. Results and Discussion

### 3.1 Brake thermal efficiency

Figure 2 presents the variations of BTE for Diesel, WPF, neat DPF, and DPF-α-terpineol blends (αT05/αT10/αT15) over 20-100% load at constant speed. For all fuels, BTE increases monotonically with load (14-43%), consistent with reduced relative heat losses and improved combustion efficiency as brake mean effective pressure rises. Diesel defines the upper envelope at each operating point, followed in order by DPF-αT15, DPF-αT10, DPF-αT05, neat DPF, and WPF. When benchmarked against Diesel, αT15 narrows but does not close the gap: at 20% load, Diesel exceeds αT15 by 4.7% relative to Diesel, widening to 5.6% at 100% load. This behavior likely reflects Diesel's higher LHV and cetane quality, which favors shorter ignition delay and more optimal heat release phasing at high load [3]. The consistent BTE uplift from α-terpineol is coherent with in-fuel oxygen, which promotes premixed burning and soot oxidation, modified spray/volatility, improving atomization and mixture preparation [16].

### 3.2 Brake specific fuel consumption

Figure 3 presents the variations of BSFC for Diesel, WPF, neat DPF, and DPF-α-terpineol blends (αT05/αT10/αT15) over 20-100% load at constant speed. BSFC decreases monotonically with load for every fuel, diesel decreases from 0.6486 to 0.2922 kg/kWh (55%), DPF from 0.6650 to 0.3500 kg/kWh (47%), and DPF-αT15 from 0.6299 to 0.3211 kg/kWh (49%). WPF exhibits the highest BSFC at all loads, Diesel the lowest, with the αT series bridging the gap between neat DPF and Diesel. Relative to DPF, the reductions are nearly loading invariant for 40-100% load and scale almost linearly with blend level. Averaged over the five loads, BSFC declines from 0.4553 kg/kWh (DPF) to 0.4458 (2.1%, αT05), 0.4344 (4.6%, αT10), and 0.4217 (7.4%, αT15); WPF averages 0.4962 kg/kWh and Diesel 0.4124 kg/kWh.

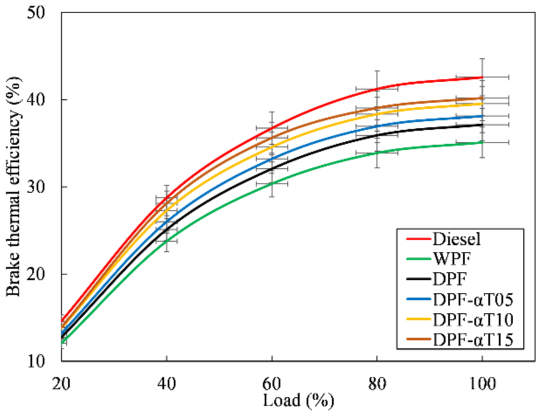


**Figure 2.** The BTE variations with respect to load for all test fuels

At 20% and 40% load, αT15 slightly outperforms Diesel on BSFC (2.9% and 0.7%, respectively). Above 60% load, Diesel regains the advantage, with αT15 higher by +3.6% (60%), +8.7% (80%), and +9.9% (100%). Importantly, αT15 closes much of DPF's penalty vs Diesel at high load. The gap at 100% load decreases from +19.8% (DPF vs Diesel) to +9.9% (αT15 vs Diesel), about a 50% reduction in deficit. At 40-60% load, the deficit is reduced by ≥70%, and at 20-40% it is eliminated.

The near linear BSFC improvement with αT fraction is consistent with better mixture preparation (viscosity/volatility) and in-fuel oxygen promoting more complete burning effects that are most effective from 40-80% load [4]. Diesel's advantage at very high load likely reflects its higher LHV and cetane, which favor shorter ignition delay and optimal heat release phasing under diffusion dominated combustion [17]. From a calibration standpoint, αT10-αT15 are preferred for fuel economy within the tested window. Further high load tuning (e.g., slight SOI/rail pressure) would likely narrow the remaining BSFC gap to Diesel without eroding the αT gains observed at mid loads.

### 3.3 Exhaust gas temperature

Figure 4 presents the variations of EGT for Diesel, WPF, neat DPF, and DPF-α-terpineol blends (αT05/αT10/αT15) over 20-100% load at constant speed. EGT increases monotonically with load for all fuels, from 125-180°C at 20% load to 485-595°C at full load. Diesel consistently exhibits the lowest EGT, WPF the highest, with neat DPF and the αT blends in between. Averaged over all loads, EGT falls from 321.4 °C (DPF) to 312.8°C (2.7%, αT05), 302.6°C (5.9%, αT10), and 293.0°C (8.8%, αT15), demonstrating a clear, monotonic dose response. The αT blends markedly close DPF's EGT gap to Diesel, especially at low to mid loads. With αT15, EGT is essentially equal to Diesel at 20% load (127 vs 126°C) and remains within 4-9% of Diesel from 40-100% load (e.g., 191 vs 184°C at 40%, 506 vs 485°C at 100%). By contrast, WPF is the warmest case at every load and approaches the common durability threshold at high load (594°C at 100%).

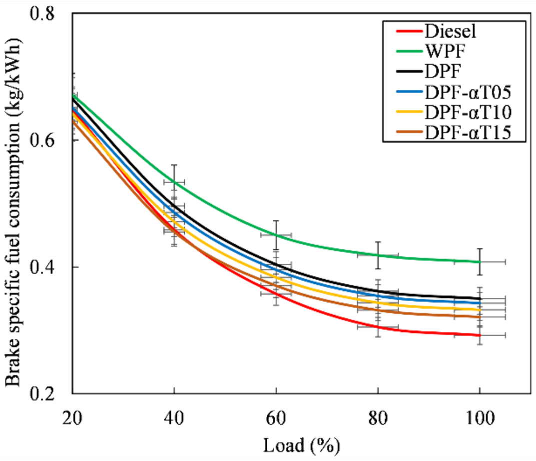


**Figure 3.** The BSFC variations with respect to load for all test fuels

Lower EGT with α-terpineol indicates reduced late cycle heat release and improved combustion efficiency, consistent with in-fuel oxygen that accelerates premixed burning and soot oxidation, and low viscosity, which enhances spray air mixing [5]. The largest percentage drops (9-11%) occur from 20-80% load, where mixture preparation is most influential. The relative benefit narrows at 100% load as diffusion burn dominates, though αT15 still trims 34°C vs DPF and halves DPF's excess over Diesel [6]. From a thermal management and robustness perspective, αT10-αT15 are preferred. They reduce EGT across the duty map, increase margin to high temperature limits, and reduce the likelihood of penalty events in risk aware objectives that incorporate EGT thresholds [18]. Targeted high load calibration could further align αT15 with Diesel while preserving its mid load advantages.

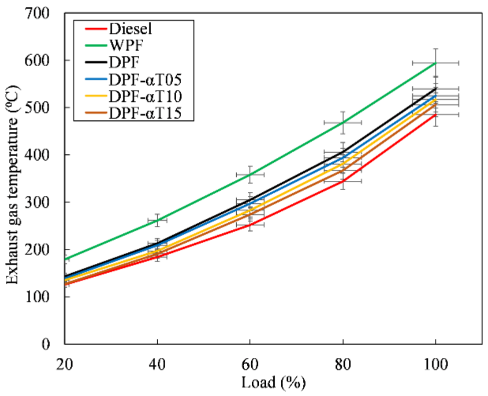


**Figure 4.** The EGT variations with respect to load for all test fuels

### 3.4 Oxides of nitrogen

Figure 5 presents the variations of NOx for Diesel, WPF, neat DPF, and DPF-α-terpineol blends (αT05/αT10/αT15) over 20-100% load at constant speed. For every fuel, NOx rises monotonically with load, reflecting higher in-cylinder temperatures and longer diffusion burn residence at high BMEP. Diesel is the lower envelope at all loads (212 to 699 ppm from 20-100%), WPF the upper (278-954 ppm), with neat DPF and the αT blends in between. Averaged over the duty map, NOx drops from 512 ppm (DPF mean) to 504 ppm (1.7%, αT05), 492 ppm (4.0%, αT10), and 474 ppm (7.4%, αT15). The absolute DPF-αT15 benefit widens with load (19.5 ppm at 20% to 58.2 ppm at 100%), while percent reduction remains in the 5-10% band. Despite the improvements, αT blends remain higher than Diesel (αT15 is +6.2%, +5.1%, +7.6%, +11.3%, +12.2% at 20-100% loads, respectively). Nevertheless, αT15 halves the DPF penalty to Diesel at high load: at 100% load, the excess over Diesel shrinks from +143 ppm (DPF) to +85 ppm (αT15).

The NOx abatement with αT is consistent with enhanced spray air mixing from reduced viscosity, and in-fuel oxygen that promotes earlier, more complete premixed burning, both suppress local stoichiometric hot zones that drive thermal NOx [11]. The simultaneous EGT decrease reported for αT blends supports a reduction in peak temperature exposure, particularly from 20-80% load where mixing dominates. The benefit narrows at 100% load as diffusion burn governs, yet αT15 still yields a substantive 58 ppm improvement vs DPF [19]. Within the risk aware objective of the present study (CVaR0.2 on load), the worst-case load is 100%, so the 6-7% NOx cut delivered by αT15 at this point materially improves tail performance. If NOx compliance is a policy priority, αT15 is the preferred DPF choice in the tested window. Additional high load calibration should further narrow the residual gap to Diesel without sacrificing the mid load NOx advantages already observed.

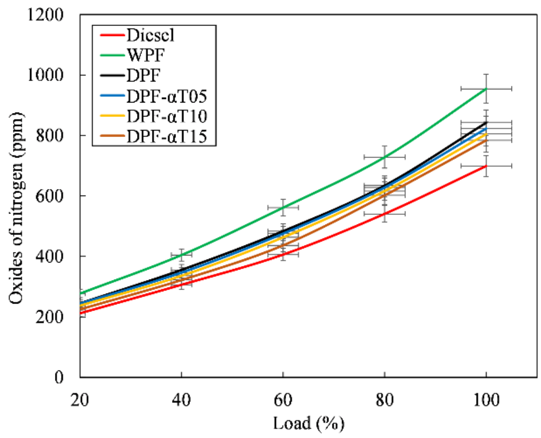


**Figure 5.** The NOx variations with respect to load for all test fuels

### 3.5 Hydrocarbon

Figure 6 presents the variations of HC for Diesel, WPF, neat DPF, and DPF-α-terpineol blends (αT05/αT10/αT15) over 20-100% load at constant speed. HC decreases monotonically with load for all fuels e.g., Diesel falls from 60.48 to 18.48 ppm (69%), DPF from 70.00 to 28.28 ppm (60%), and WPF from 75.60 to 38.08 ppm (50%). At every load the ordering is Diesel< DPF-αT15< DPF-αT10< DPF-αT05< DPF< WPF, i.e., α-terpineol consistently suppresses HC relative to neat DPF. Averaged over the duty map, HC drops from 42.67 ppm (DPF) to 40.77 ppm (4.5%, αT05), 38.19 ppm (10.5%, αT10) and 35.73 ppm (16.3%, αT15), confirming a clear dose response. Diesel remains the cleanest case, but αT15 closes most of DPF's gap to Diesel. On average, DPF exceeds Diesel by +36.6%, whereas αT15 is only +14.3% above Diesel i.e., αT15 eliminates about 61% of DPF's HC penalty. Per load, αT15 is within 7-25% of Diesel (e.g., 21.28 vs 18.48 ppm at 100% load), while greatly undercutting neat DPF and WPF.

The HC reduction with α-terpineol is consistent with enhanced oxidation of fuel rich pockets and late cycle residuals due to oxygenated chemistry, together with improved mixture preparation supported by the measured decrease in blend viscosity relative to neat DPF [20]. Better atomization and reduced wall wetting tendency suppress the formation of quench layer hydrocarbons and unburned fuel films, which is particularly relevant at light-to-mid loads where flame temperatures and oxidation rates are intrinsically less [1]. The increasing percentage benefit toward 40- 100% load further suggests that α-terpineol helps mitigate incomplete burn pathways that intensify under higher fueling rates, narrowing the HC penalty of DPF relative to diesel.

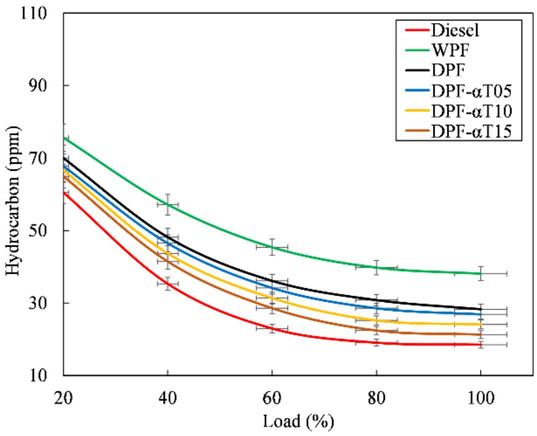


**Figure 6.** The hydrocarbon variations with respect to load for all test fuels

### 3.6 Carbon monoxide

Figure 7 presents the variations of CO for Diesel, WPF, neat DPF, and DPF-α-terpineol blends (αT05/αT10/αT15) over 20-100% load at constant speed. CO remains low and fairly flat from 20-80% load for all fuels (0.22-0.31 %vol), then rises at 100% load as diffusion burning and local oxygen deficit increase. At every load WPF is the highest case CO, Diesel the lowest, with neat DPF and the αT blends in between. αT addition reduces CO at each load, with a clear dose response and the largest gains at high load. At 20-60% load, CO values are essentially indistinguishable from DPF within two decimals (0.29/0.26/0.23 %vol), indicating a measurement floor regime where mixture oxidation is already near complete. At 80% load, αT15=0.22 %vol vs DPF=0.23 %vol (4.3%), for αT10 and αT05 closely at 0.23%vol. At 100% load, for αT05=0.50 (3.8%), αT10=0.48 (7.7%), αT15=0.46 (11.5%) relative to DPF=0.52 %vol. At 80% load the best blend (αT15=0.22 %vol) is marginally below Diesel (0.23 %vol). At 100% load, αT15 is very close to Diesel (0.46 vs 0.45 %vol), substantially narrowing DPF's high load penalty (0.52 to 0.46 i.e., 50% reduction in the excess over Diesel).

CO reductions with α-terpineol are consistent with improved spray air mixing and in-fuel oxygen accelerating burnout of rich pockets, especially impactful at high load, where diffusion limited regions dominate. The near coincidence of values at low/mid loads reflects a floor set by oxidation completeness under the fixed speed, warm up conditions [21]. For CO control within the tested window, αT10-αT15 are preferred, with αT15 delivering the strongest and most load robust benefit and effectively matching diesel on the load averaged basis. If further high load reduction is targeted, a light SOI retard/EGR increase or rail pressure trim at 100% load would likely erase the residual 0.01-0.02 %vol gap to diesel without compromising the mid load gains.

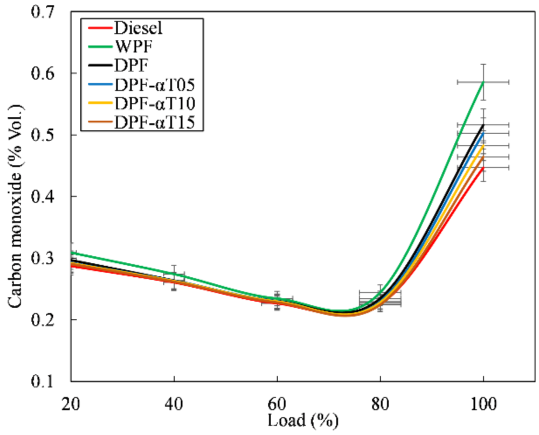


**Figure 7.** The CO variations with respect to load for all test fuels

### 3.7 Carbon dioxide

Figure 8 presents the variations of CO2 for Diesel, WPF, neat DPF, and DPF-α-terpineol blends (αT05/αT10/αT15) over 20-100% load at constant speed. CO2 rises strongly with load for all fuels consistent with higher fuel air throughput and more complete oxidation at elevated cylinder temperatures. Diesel spans 2.21 to 9.88 %vol (20 to 100% load), WPF 2.13 to 6.40 %vol, and neat DPF 2.17 to 8.02 %vol. Adding α-terpineol increases exhaust CO2 at every load in a clear, dose dependent manner, indicating enhanced conversion of fuel carbon to CO2 (and, correspondingly, less CO/HC). Relative to neat DPF, the αT15 blend raises CO2 by +11.5% (20%), +15.7% (40%), +29.8% (60%), +50.3% (80%), and +47.1% (100%) (e.g., 8.02 to 11.80 %vol at full load). The intermediate blends follow the same monotone trend: αT10 (2.38/ 2.65/ 3.37/ 6.92/ 10.63%vol) and αT05 (2.33/ 2.60/ 3.31/ 6.78/10.41%vol) lie between DPF and αT15 at all loads. On a duty map average, CO2 increases from 4.11%vol (DPF) to 5.09 (αT05), 5.19 (αT10), and 5.67%vol (αT15), a 38% rise from DPF to αT15. Diesel's CO2 is lower than any DPF-αT blend at all loads (e.g., 9.88%vol vs 11.80%vol for αT15 at 100% load). Averaged across loads, Diesel is 4.82%vol, so αT15 is 18% higher in volume fraction terms. The upward shift in CO2 aligns with the observed reductions in CO and HC for αT blends i.e., more complete oxidation of carbon. It also tracks with lower BSFC and higher BTE. Even if the exhaust CO2 fraction is higher, the fuel mass per kWh is lower, so the tailpipe CO2 mass per kWh does not necessarily increase proportionally [22]. The upward shift in CO2 for the α-terpineol blends could be interpreted together with the simultaneous CO and HC reductions. Larger fractions of fuel carbon is driven toward complete oxidation rather than partial oxidation products [17]. This is consistent with oxygenated functionality introduced by α-terpineol that facilitates oxidation chemistry in locally rich zones, and improved mixture preparation inferred from the measured viscosity reduction of the DPF-α-terpineol blends relative to neat DPF. This promotes finer atomization and more uniform air-fuel mixing [1]. The effect becomes most visible at 60-100% load, where diffusion burning dominates and incomplete burnout pathways are otherwise amplified.

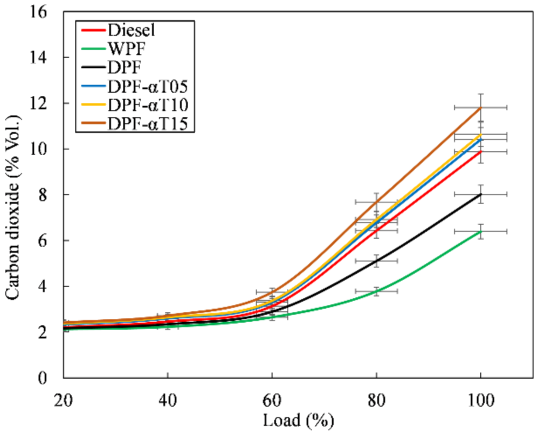


**Figure 8.** The CO2 variations with respect to load for all test fuels

### 3.8 Smoke

Figure 9 presents the variations of smoke emission for Diesel, WPF, neat DPF, and DPF-α-terpineol blends (αT05/αT10/αT15) over 20-100% load at constant speed. Smoke emission increases monotonically with load for all fuels, reflecting greater diffusion controlled burning and residence time at high BMEP [16]. Diesel remains the cleanest case at each point (16.75 to 45.84% opacity from 20 to 100% load), WPF demonstrates highest smoke (21.71-58.71%), with neat DPF and the αT blends in between. Averaged across the duty map, smoke falls from 34.69% (DPF) to 34.19% (αT05, 1.4%), 33.36% (αT10, 3.8%), and 32.46% (αT15, 6.4%), confirming a clear dose response. WPF averages 39.05%, whereas Diesel averages 29.79%. Although αT blends do not fully match diesel, αT15 narrows DPF's excess smoke by 60% on an average basis: DPF is +16.5% above Diesel, while αT15 is +9.0%. At full load, the most critical point for risk aware objectives αT15 reduces 2.57% from DPF (52.28-49.71%), materially reducing worst case opacity.

The opacity reductions with α-terpineol are consistent with two coupled effects, oxygenated blending promotes soot oxidation and weakens soot persistence in late cycle diffusion, under oxygen deficit conditions at higher load [19]. The measured reduction in blend viscosity relative to neat DPF supports improved spray breakup and air-fuel mixing, which reduces the formation of locally over rich pockets that seed soot inception and growth [16]. The persistence of the benefit up to 100% load indicates that α-terpineol acts not only as a chemical oxygen carrier but also as a practical mixing conditioner for DPF, yielding a coherent response behavior.

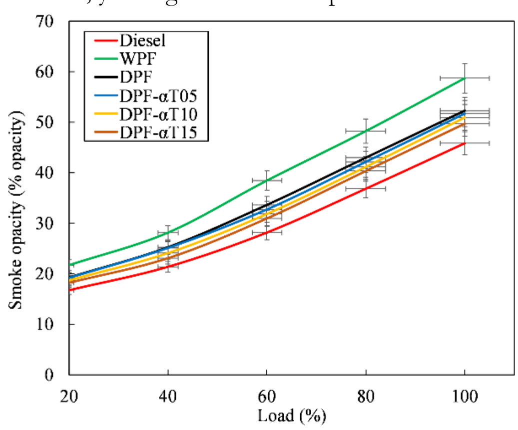


**Figure 9.** The smoke variations with respect to load for all test fuels

### 3.9 Risk aware multi objective optimization

Each raw metric is transformed by a quantile calibrated sigmoid desirability (anchors at q_0.2, q_0.5, q_0.8), per load performance is the geometric mean across metrics, cross load robustness is the CVaRα of those per load scores. The baseline uses α=0.20, exponent weights ϱ_j giving added emphasis to NOx and smoke, and no penalty terms.

#### 3.9.1 Baseline ranking and worst load diagnosis

Using the baseline configuration of the framework (quantile calibrated desirability; geometric mean across metrics; CVaR0.2 across loads), the Baseline risk aware ranking across fuels CVaR@0.2 (geometric desirability) with 95% bootstrap confidence intervals is presented in Fig. 10. Diesel shows the highest risk aware score (CVaR0.2=0.242), and WPF the lowest (0.081). Within the DPF family the scores increase monotonically with α-terpineol content, DPF-αT15=0.197> DPF-αT10=0.177> DPF-αT05=0.157> DPF=0.141. Relative to neat DPF, the improvement in the worst load performance is substantial +11% (αT05), +26% (αT10), and +40% (αT15). The remaining gap to Diesel is modest for the best blend (αT15 is 0.045 CVaR units lower; 23% of αT15's score), while WPF underperforms DPF by 43%, confirming the benefit of the DPF route and the α-terpineol co-blend.

Bootstrap confidence intervals (Table 5) indicate non overlap between αT15 and neat DPF [0.197,0.476] vs [0.141,0.387], and only partial overlap with αT10 [0.177,0.453]. Thus, the top rank of αT15 within the DPF family is statistically stable at the present grid. With five loads and α=0.20, the CVaR tail contains one load (k=1). For all DPF family fuels, the 100% load consistently enters the tail, identifying full load operation as the dominant robust limiter. This is mechanistically coherent with diffusion controlled burning and higher thermal stress at peak load, where smoke, CO, EGT aref most challenging.

Because CVaR is governed by the worst-case point, small, targeted calibration at 100% load e.g., a slight SOI retard, modest EGR, or a rail pressure/boost trim offers the highest leverage to lift the risk aware score, especially for neat DPF and αT05 [23]. Conversely, αT15 combines strong average behavior with superior worst load performance, explaining its consistent lead in Fig. 10 and Table 5

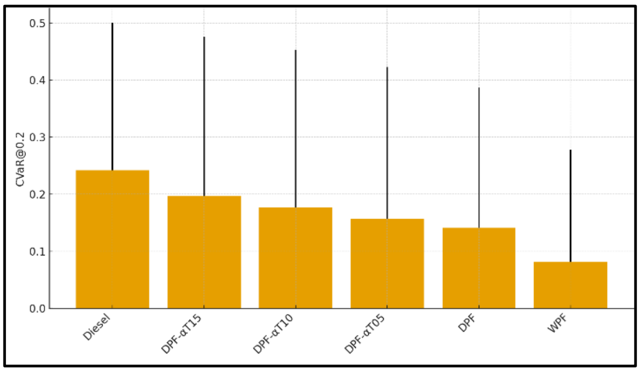


**Figure 10.** Baseline risk aware ranking across fuels: CVaR@0.2 (geometric desirability) with 95% bootstrap confidence intervals

**Table 5.** Baseline CVaR@0.2 scores by fuel with 95% bootstrap confidence intervals and worst load membership

| Fuel | CVaR@0.2 | 95% CI (low-high) |
|---|---|---|
| Diesel | 0.242 | 0.242-0.501 |
| DPF-αT15 | 0.197 | 0.197-0.476 |
| DPF-αT10 | 0.177 | 0.177-0.453 |
| DPF-αT05 | 0.157 | 0.157-0.423 |
| DPF | 0.141 | 0.141-0.387 |
| WPF | 0.081 | 0.081-0.278 |

### 3.9.2 CVaR vs α-terpineol blend fraction

Figure 11 demonstrates the risk aware score responds to the α-terpineol treat rate in DPF. The CVaR0.2 increases monotonically across the tested window, with an almost linear rise from 0.141 (0%) →0.157 (5%) →0.177 (10%) →0.197 (15%). Each 5-point increment yields a meaningful gain in worst-load robustness +11% at 5%, +26% at 10%, and +40% at 15% relative to neat DPF. The step sizes are consistent (+0.016 to +0.020 CVaR units per 5% α-terpineol), indicating that the additive improves multiple metrics concordantly at the load that governs CVaR (100% load). Because CVaR averages the worst operating point, the upward trend implies that α-terpineol strengthens the blend precisely where diffusion burn and thermal stress are greatest. Mechanistically, this is coherent with the observed increases in BTE and reductions in BSFC, smoke, CO/HC, EGT. The multiplicative per load aggregation then compounds these improvements into a higher tail score [23].

Within 0-15 vol.%, the optimum is at the boundary (15%), there is no interior maximum in the measured range. If properties and operability permit, a follow-on sweep (e.g., 12-18%) would determine whether the CVaR curve bends toward a plateau or continues to rise. In the absence of those data, 15% α-terpineol is the data supported choice for risk-aware operation, while 10% remains a close, operationally attractive alternative (supply/cold flow). Any move beyond the current window should be evaluated against property constraints (flash point, viscosity, miscibility, lubricity) and the same CVaR protocol to preserve comparability.

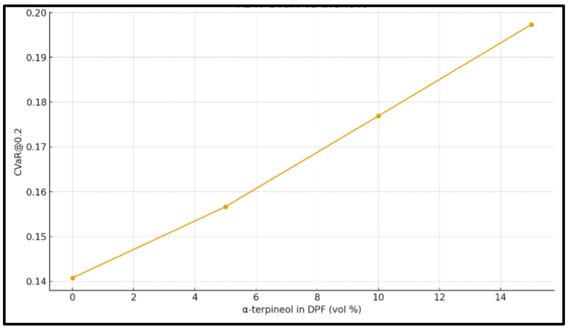


**Figure 11.** Risk aware performance versus α-terpineol treat rate in DPF: CVaR@0.2 as a function of blend fraction (0-15 vol%)

### 3.9.3 Risk aversion sensitivity

Figure 12 examines the risk aware score changes as the CVaR level α is swept from 0.15 to 0.35 while keeping metric weights at their baseline values. Across the entire sweep, the ordering of the DPF family is unchanged DPF-αT15> DPF-αT10> DPF-αT05> DPF with diesel remaining the upper envelope and WPF the lower. The curves are near parallel, indicating that the preference for α-terpineol is robust to the decision maker tolerance for worst case performance.

The interpretability of α is clear in this dataset with five loads for α=0.15-0.20, the tail size is k=⌈αL⌉=1, so only the single worst load contributes to CVaR for α≥0.25, the tail expands to two loads. As α increases, the curves increase slightly in favor of the α-terpineol blends because the optimization puts more weight on heavy load operation, where α-terpineol most strongly reduces smoke, CO, EGT. In other words, greater risk aversion accentuates the advantages already visible at full load and, at α≥0.25, also at the next worst load [22].

Since policy or fleet priorities may vary, α provides a transparent knob, lower α (closer to a worst-point view) and higher α (averaging the worst couple of points) both select DPF-αT15, with DPF-αT10 a consistent, near optimal alternative. This stability reflects a structural improvement in the tail behavior of the α-terpineol blends.

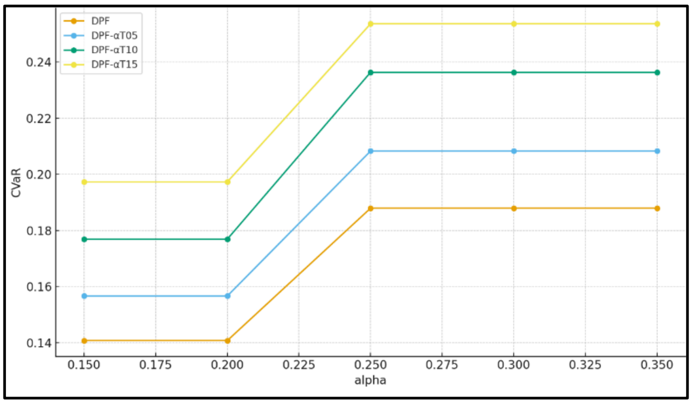


**Figure 12.** Risk aversion sweep: CVaR@α as a function of α (0.15-0.35) for Diesel, WPF, DPF, and DPF-αT blends

### 3.9.4 Weight sensitivity

Figure 13 quantifies the relative ranking changes when the desirability exponent of each metric, ϱ_j, is perturbed one at a time by +0.3 from the baseline while all other weights are held fixed. The change in the score gap ΔCVaR=CVaR(DPF-αT15)-CVaR(DPF-αT10). Positive bars therefore indicate conditions that reinforce the preference for the 15% blend, and the negative bars would indicate conditions that erode it. The largest positive leverage arises from NOx and smoke weights. Up weighting either metric widens ΔCVaR, because DPF-αT15 achieves the biggest tail-load reductions in NOx and smoke, and CVaR emphasizes the worst load where these advantages are most pronounced [24]. Increasing BTE (and, to a lesser degree, down weighting BSFC by raising its importance) also increases the gap, reflecting the broadly higher efficiency / lower BSFC of the α-terpineol blends across the map. The effect is smaller than NOx/smoke but directionally consistent. Weights on CO, HC, EGT, and CO2 have modest influence on the αT15-αT10 separation within the tested range, and they do not materially alter the ordering. Crucially, no single weight perturbation within Δϱ =+0.3 flips the DPF-family ranking. DPF-αT15 remains the best, DPF-αT10 remains second. This indicates the preference for αT15 is not an artifact of a narrow weighting scheme but reflects a concordant improvement across the metrics that dominate the tail (particularly emissions at full load) [25]. From a policy standpoint, if the decision maker prioritizes air quality compliance (higher NOx/smoke weights), the case for αT15 strengthens further. If economy is emphasized (higher BTE/BSFC weights), αT15 again retains the lead, with αT10 a near optimal operational alternative.

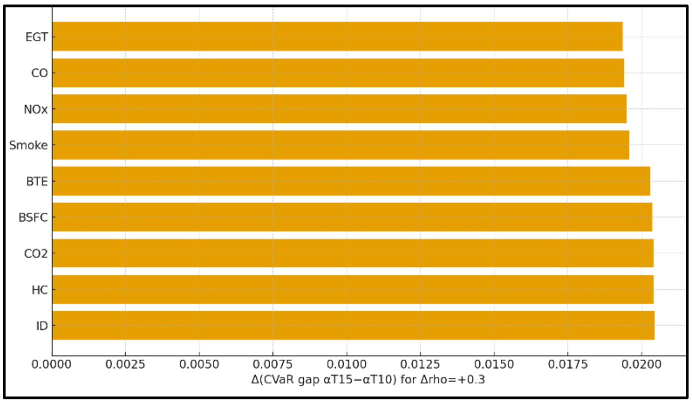


**Figure 13.** Weight sensitivity (tornado): change in CVaR@0.2 gap DPF-αT15-DPF-αT10 under a +0.3 one-at-a-time perturbation of each desirability exponent ϱ_j

### 3.9.5 Objective flavor comparisons

The risk aware scores under three decision "flavors" policy lean (greater weight on regulated emissions), economy lean (greater weight on efficiency), and robustness lean (soft penalties for constraint exceedances). Table 6 lists the corresponding CVaR values. In all cases, the DPF-α-terpineol order is strict and stable: DPF-αT15> DPF-αT10> DPF-αT05> DPF. Under policy-lean (NOx/ smoke up weighted; α=0.30), DPF-αT15 achieves the highest tail performance (0.239), followed by αT10 (0.222), αT05 (0.195), and neat DPF (0.176). The uplift reflects α-terpineol larger NOx and smoke reductions at high load, the point that dominates CVaR as α rises and the tail expands to include the two worst loads. Diesel remains the upper envelope and WPF trails all fuels. Under economy lean (BTE/BSFC up weighted; α=0.20). Efficiency emphasis preserves the ordering (αT15=0.223> αT10=0.201> αT05=0.178> DPF=0.160). Gains arise from monotonic BTE/BSFC across loads for the α-terpineol blends, which compound multiplicatively in the per load desirability and carry into CVaR. Under robustness lean (baseline weights; α=0.20+soft penalties for EGT>600 °C). αT15 leads (0.197) over αT10 (0.177), αT05 (0.157), and DPF (0.141). The advantage is driven by lower EGT for αT≥10%, which avoid penalties at light and mid loads and full load (EGT), improving the worst-case average. Across flavors, αT15 is the recommended DPF-family blend. αT10 is a near optimal alternative when supply, cost, or cold flow constraints favor a lower treat rate. The persistence of the ranking under materially different weightings and tail definitions indicates that the superiority of α-terpineol is not a weighting artifact but the result of concordant improvements in the metrics that govern worst load behavior [23].

**Table 6.** Objective flavor comparison: CVaR scores by fuel under policy lean (α=0.30), economy lean (α=0.20), and robustness lean (α=0.20 + penalties) configurations, with winner and rationale

| Flavor (α) | DPF | DPF-αT05 | DPF-αT10 | DPF-αT15 | Winner & rationale |
|---|---|---|---|---|---|
| Policy lean (0.30) | 0.18 | 0.195 | 0.222 | 0.239 | αT15: largest NOx/smoke relief at tail |
| Economy lean (0.20) | 0.16 | 0.178 | 0.201 | 0.223 | αT15: BTE↑ and BSFC↓ across map |
| Robustness lean (0.20 + penalties) | 0.14 | 0.157 | 0.177 | 0.197 | αT15: avoids EGT penalties |

### 3.9.6 Desirability calibration sanity check

Figure 14 validates the mapping from raw metrics (heterogeneous units, mixed directions) to unitless desirability used by optimization. Each metric y_j is transformed by a quantile calibrated logistic function anchored at its sample quantiles (q_0.2, q_0.5, q_0.8). The slope is set as k_j, so that the median maps to d=0.5 and, approximately, q_0.2↦0.25 and q_0.8↦0.75. This choice makes the transformation scale free and robust to outliers (quantiles, not extrema), preserves monotonicity in the correct sense (e.g., BTE is increasing; BSFC/ NOx/ Smoke/ CO/ HC/ EGT/ CO2 are decreasing), and ensures comparable dynamic range across metrics before the geometric aggregation per load. No single metric can dominate solely because it is measured on a larger numeric scale [23]. Figure 14 (shown for BTE and NOx) illustrate two properties that matter for optimization accuracy. First, most observations fall on the steep central portion of each S-curve rather than saturating at d≈0 or d≈1. Hence, improvements (or regressions) remain visible to the objective instead of being clipped. Second, increasing BTE increases desirability smoothly, while increasing NOx lowers it smoothly, with similar "effective leverage" between the 20th and 80th percentiles across both metrics. This balanced leverage allows the multiplicative per load desirability to reward concordant improvements (e.g., BTE↑ and NOx↓ together) without overweighting either axis.

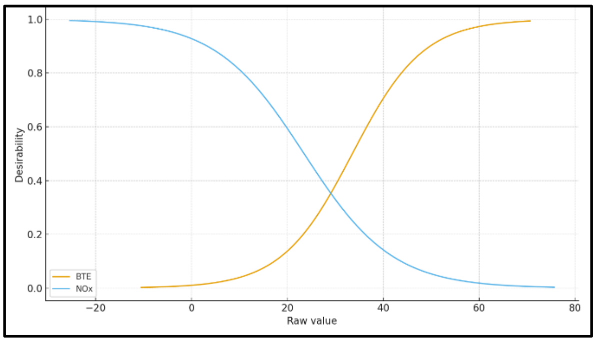


**Figure 14.** Desirability calibration: quantile anchored logistic mappings (q20-q50-q80) from raw metrics to unitless desirability, with example curves for BTE (maximize) and NOx (minimize).

## 4. Limitations of the Study

This study has several limitations that bound the interpretation and generalizability of the results:

The analysis uses five steady state loads at a single speed. With α=0.20, CVaR's tail contains only one point, so worst-case performance is effectively determined by the 100% load. A denser grid (more loads and additional speeds) would stabilize tail estimates and could reveal load speed interactions that are invisible here.

Injection timing, rail pressure, EGR, and boost were held fixed (or only minimally adjusted) when comparing fuels. As a result, each blend is not operating at its own calibration optimum; differences partly reflect calibration mismatch rather than pure fuel effects. A fair "best effort" comparison would include per fuel micro tuning, ideally constrained by the same emissions/thermal limits.

The quantile anchored logistic mapping (q20-q50-q80) is data adaptive to this experiment. Adding or removing fuels (or changing the operating map) would shift anchors and can re-scale desirability. While this is appropriate within study, cross study comparability would require either frozen anchors or explicit re-calibration is required.

Although weight sweeps and objective "flavors" were explored, the chosen exponent ranges and robustness thresholds (EGT≤600°C) are illustrative. Different regulatory priorities, safety margins, or hardware limits could motivate alternative weight/threshold settings and alter absolute scores.

## 5. Conclusions

This study demonstrated a risk aware, multi objective methodology for selecting diesel plastic fuel blends with an alcoholic oxygenate (α-terpineol) across the duty map of a CRDi diesel engine. Heterogeneous responses (BTE, BSFC, NOx, CO, CO2, HC, smoke, EGT) were mapped via quantile anchored logistic desirability and aggregated per load (geometric mean), with CVaR across loads to emphasize worst case behavior. The method yields transparent, policy tunable decisions that remain stable under risk aversion and weighting sweeps, pinpointing full load operation as the dominant limiter and elevating α-terpineol co-blends. The key findings are as follows:

The Risk aware ranking is obtained as, Diesel (0.242) > DPF-αT15 (0.197) > DPF-αT10 (0.177) > DPF-αT05 (0.157) > DPF (0.141) > WPF (0.081). Relative to neat DPF, worst-load performance improves by +11% (αT05), +26% (αT10), +40% (αT15); 100% load consistently forms the CVaR tail.

Considering the blend fraction effect, CVaR rises monotonically with α-terpineol: 0.141/ 0.157/ 0.177/ 0.197 for 0/ 5/ 10/ 15 vol%, i.e., +0.016-0.020 CVaR units per 5 vol% step and no interior optimum within 0-15 vol%.

Average BSFC drops from 0.4553 to 0.4217 kg/kWh (7.4%) for αT15. At 100% load the Diesel-DPF gap is roughly halved (DPF 0.52 vs αT15 0.46 %vol CO).

Average EGT falls 321.4 to 293.0°C (8.8%) for αT15 and at 100% load αT15 reduces 34°C vs DPF (506 vs 540°C), enlarging thermal margin.

Mean HC decreases from 42.67 to 35.73 ppm (16.3%) for αT15, while αT15 reduces 61% of DPF's average HC excess vs Diesel.

At 100% load, CO falls from 0.52 to 0.46 %vol (11.5%) for αT15, essentially matching Diesel (0.45 %vol) and at low/mid loads are near the baseline.

Average smoke reduces from 34.69 to 32.46% opacity (6.4%) for αT15 and at full load, opacity drops from 52.28 to 49.71%, materially improving the tail pipe smoke.

Within the tested window, 15 vol% α-terpineol in DPF is the risk aware first choice, and 10 vol% is a near optimal operational alternative. Because CVaR is driven by the worst case (100%) load, the most effective levers to raise robustness are targeted high load, which further depress EGT, and reduce smoke/CO without sacrificing mid load gains. The overall recommendation is method stable, holding across risk aversion levels (α-sweep) and metric weightings (policy/economy/robustness flavors). Future work should broaden both the operating envelope and the methodological rigor. Experimentally, a denser load speed matrix and transient drive cycles are needed to stabilize tail estimates beyond a single worst point and to capture mixing/after treatment dynamics under real duty. Each blend should be re-evaluated under per fuel micro calibration (timing/rail pressure/EGR/boost) within common constraints to decouple fuel effects from calibration mismatch.

## 6. References:


[1] G. N. Kannaiyan, B. Pappula, and S. Makgato, "Experimental investigation on addition of furfuryl alcohol to diesel plastic fuel blends and optimization using kissing numbers," Sci. Rep., vol. 15, no. 1, p. 20672, 2025. https://doi.org/10.1038/s41598-025-07174-4

[2] J. Hunicz et al., "Waste plastic pyrolysis oils as diesel fuel blending components: Detailed analysis of combustion and emissions sensitivity to engine control parameters," Energy, vol. 313, p. 134093, 2024. https://doi.org/10.1016/j.energy.2024.134093

[3] H. Yaqoob, H. M. Ali, U. Sajjad, and K. Hamid, "Investigating the potential of plastic pyrolysis oil-diesel blends in diesel engine: Performance, emissions, thermodynamics and sustainability analysis," Results Eng., vol. 24, p. 103336, 2024. https://doi.org/10.1016/j.rineng.2024.103336

[4] D. Kim, J. Yang, and J. Kwon, "Performance and emission characteristics of n-pentanol-diesel blends in a single-cylinder CI engine," Energies, vol. 18, no. 19, p. 5083, 2025. https://doi.org/10.3390/en18195083

[5] T. Pachiannan, W. Zhong, D. Balasubramanian, M. A. Alshehri, A. Pugazhendhi, and Z. He, "Enhancing engine performance, combustion, and emission characteristics through hydrogen enrichment in n-pentanol/diesel blends," Int. J. Hydrogen Energy, vol. 98, pp. 741-750, 2025. https://doi.org/10.1016/j.ijhydene.2024.12.005

[6] M. Bhowmik, M. Deb, and G. Sastry, "Performance and emission assessment of an indirect ignition diesel engine fuelled with waste plastic pyrolysis oil and ethanol blends," Front. Therm. Eng., vol. 5, p. 1548806, 2025. https://doi.org/10.3389/fther.2025.1548806

[7] N. Grozdanić, M. Kijevčanin, and I. Radović, "Terpene-based biofuel additives (citral, limonene, and linalool) with chloroform: Experimental and modeling study of volumetric and transport properties," Processes, vol. 13, no. 4, p. 974, 2025. https://doi.org/10.3390/pr13040974

[8] T. Bierkandt, N. Gaiser, J. Bachmann, P. Oßwald, and M. Köhler, "Terpene speciation: Analytical insights into oxidation and pyrolysis of limonene and 1,8-cineole via molecular-beam mass spectrometry," Combust. Flame, vol. 272, p. 113854, 2025. https://doi.org/10.1016/j.combustflame.2024.113854

[9] O. I. Awad et al., "Combustion and emission analysis of $NH_3$-diesel dual-fuel engines using multi-objective response surface optimization," Atmosphere, vol. 16, no. 9, p. 1032, 2025. https://doi.org/10.3390/atmos16091032

[10] M. Elkelawy et al., "Predictive modeling and optimization of a waste cooking oil biodiesel/diesel powered CI engine using RSM with central composite design," Sci. Rep., vol. 14, no. 1, p. 30474, 2024. https://doi.org/10.1038/s41598-024-77234-8

[11] G. Jia et al., "Multi-objective optimization of emission parameters of a diesel engine using oxygenated fuel and pilot

injection strategy based on RSM-NSGA III," Energy, vol. 293, p. 130661, 2024. https://doi.org/10.1016/j.energy.2024.130661

[12] D. Xi, L. Jiang, J. Cui, X. Sun, and W. Long, "Fuel economy-emission trade-off optimization for diesel/natural gas dual-fuel engine using many-objective many-population hybrid genetic algorithm," Energy, p. 137347, 2025. https://doi.org/10.1016/j.energy.2025.137347

[13] C. Özgür, E. Uludamar, H. S. Soyhan, and R. M. Raja Ahsan Shah, "Optimisation of exhaust emissions, vibration, and noise of unmodified diesel engine fuelled with canola biodiesel-diesel blends with natural gas addition using response surface methodology," 2024. https://doi.org/10.2516/stet/2024031

[14] M. Selvam, N. Pragadish, K. Harish, R. G. Srinivasan, Y. Devarajan, and N. Kaliappan, "Investigating emission characteristics and combustion performance of a CRDI engine utilizing biodiesel derived from waste cooking oil and pentanol blends," Sci. Rep., vol. 15, no. 1, pp. 1-16, 2025. https://doi.org/10.1038/s41598-025-98462-6

[15] M. K. Jamil et al., "Multi-objective RSM-based optimization of diesel-diethyl ether blends in diesel engine to achieve sustainable development goals," Case Stud. Therm. Eng., vol. 59, p. 104542, 2024. https://doi.org/10.1016/j.csite.2024.104542

[16] P. Bridjesh, P. Periyasamy, A. V. K. Chaitanya, and N. K. Geetha, "MEA and DEE as additives on diesel engine using waste plastic oil-diesel blends," Sustain. Environ. Res., vol. 28, no. 3, pp. 142-147, 2018. https://doi.org/10.1016/j.serj.2018.01.001

[17] S. Ellappan and B. Pappula, "Utilization of unattended waste plastic oil as fuel in low heat rejection diesel engine," Sustain. Environ. Res., vol. 29, p. 2, 2019. https://doi.org/10.1186/s42834-019-0006-7

[18] C. Ravikiran, M. S. Chandra, M. Nagappan, J. Babu, R. R. Kumar, and S. R. Ahammed, "Performance analysis of a DI diesel engine using Prosopis juliflora biodiesel in conjunction with hydrogen fuel," Int. J. Vehicle Struct. Syst., vol. 16, no. 1, 2024. https://doi.org/10.4273/ijvss.16.1.12

[19] L. Chybowski et al., "Content of selected compounds in the exhaust gas of a naturally aspirated CI engine fueled with diesel-tire pyrolysis oil blend," Energies, vol. 18, no. 10, p. 2621, 2025. https://doi.org/10.3390/en18102621

[20] N. K. Geetha and B. Pappula, "Integrated AHP and WED based approach to select optimal combination of operating parameters on spark ignition engine," SAE Tech. Paper, 0148-7191, 2019. https://doi.org/10.4271/2019-01-0025

[21] V. Ayyakkannu, T. Raja, E. Thangapandian, and V. Malaiperumal, "Synergistic impacts of calcium oxide nanoparticles infused palm seed oil biodiesel blends: CI engine efficiency and downsizing emissions," Fuel, vol. 384, p. 134066, 2025. https://doi.org/10.1016/j.fuel.2024.134066

[22] D. Madhuvanesan and J. Babu, "Optimization and prediction of performance and emission characteristics of a CRDI diesel engine fueled with waste plastic oil using RSM and ANN," Combust. Theory Model., pp. 1-20, 2025. https://doi.org/10.1080/13647830.2025.2522085

[23] F. Liu, J. Duan, C. Wu, and Q. Tian, "Risk-averse distributed optimization for integrated electricity-gas systems considering uncertainties of wind-PV and power-to-gas," Renew. Energy, vol. 227, p. 120358, 2024. https://doi.org/10.1016/j.renene.2024.120358

[24] P. Mishra et al., "Experimental assessment and optimization of the performance of a biodiesel engine using response surface methodology," Energy Sustain. Soc., vol. 14, no. 1, p. 28, 2024. https://doi.org/10.1186/s13705-024-00447-2

[25] V. V. Kannan et al., "Artificial intelligence-based prediction and multi-objective RSM optimization of Tectona grandis biodiesel with Elaeocarpus ganitrus," Sci. Rep., vol. 15, no. 1, p. 3833, 2025. https://doi.org/10.1038/s41598-025-87640-1

## Nomenclature

| | |
|---|---|
| BSFC | Brake specific fuel consumption |
| BTE | Brake thermal efficiency |
| CI | Confidence intervals |
| CO | Carbon monoxide |
| CO2 | Carbon dioxide |
| CRDi | Common rail direct injection |
| CVaR | Conditional Value-at-Risk |
| DPF | Diesel plastic fuel (50 vol.% diesel + 50 vol.% WPF) |
| DPF-αT05 | 95 vol.% DPF+5 vol.% α-terpineol |
| DPF-αT10 | 90 vol.% DPF+10 vol.% α-terpineol |
| DPF-αT15 | 85 vol.% DPF+15 vol.% α-terpineol |
| EGR | Exhaust gas recirculation |
| EGT | Exhaust gas temperature |
| HC | Hydrocarbon |
| LHV | Lower heating value |
| NOx | Oxides of nitrogen |
| RSM | Response Surface Methodology |
| WPF | Waste plastic oil/fuel |
| $d_j$ | The desirability score |
| $\bar{d}_j(y)$ | The per load aggregate desirability |
| $D_1, D_2, \ldots, D_L$ | The order statistics of load |
| $D_{geo}$ | Geometric mean of metric level desirability |
| J, J | The index response metrics set |
| $k(x)$ | The knee score |
| $k_j$ | The slope for quantile |
| l, L | The index engine loads |
| $m(x)$ | The expected metric values |
| n | The number of repeats |
| $q_{0.2}, q_{0.5}, q_{0.8}$ | The quantiles |
| $p_m$ | The penalty metric |
| $P(x,l)$ | The overall penalty |
| $s_y$ | The standard deviation |
| $u_a(y)$ | Type A standard uncertainty |
| $u_b(y)$ | Type B standard uncertainty |
| $u_c(y)$ | The combined standard uncertainty |
| x | The blend level |
| X | The fuel blend set |
| y | The measured quantity |
| $y_j(x,l)$ | The steady state mean of metric |

| | |
|---|---|
| z^ut | The ideal point in Pareto |
| z^na | The normalized distance |
| α | The level of value at risk |
| ϱ_j | The exponent weight |
| τ_m | The upper threshold |

## Appendix:

For DPF-αT15 at 100% load, BTE = 40.18%, BSFC = 0.321 kg/kWh, EGT=506°C, NOx = 784.2 ppm, HC = 21.28 ppm, CO = 0.464 vol.%, CO2 = 11.80 vol.%, Smoke = 49.71 % opacity. After applying the quantile desirability mapping, the corresponding desirability at this operating point are:

**Table A1.** Metric-by-metric desirability and contributions (DPF-αT15 at 100% load)

| Metric | Dir. | Measured ($y_i$) | $q_{0.2}$ | $q_{0.5}$ | $q_{0.8}$ | $\rho_j$ | $d_j$ | $\bar{d}_j$ | $ln\bar{d}_j$ |
|---|---|---|---|---|---|---|---|---|---|
| BTE | Max | 40.18 | 21.93 | 33.55 | 38.16 | 1.10 | 0.71 | 0.69 | -0.38 |
| BSFC | Min | 0.32 | 0.34 | 0.41 | 0.55 | 1.00 | 0.71 | 0.71 | -0.34 |
| EGT | Min | 506.00 | 183.01 | 290.00 | 471.40 | 1.00 | 0.16 | 0.16 | -1.82 |
| $NO_x$ | Min | 784.20 | 300.69 | 469.60 | 704.88 | 1.30 | 0.15 | 0.09 | -2.44 |
| HC | Min | 21.28 | 24.98 | 35.70 | 57.79 | 1.00 | 0.72 | 0.72 | -0.32 |
| CO | Min | 0.46 | 0.23 | 0.26 | 0.34 | 1.00 | 0.02 | 0.02 | -4.15 |
| $CO_2$ | Min | 11.80 | 2.37 | 3.22 | 7.07 | 1.00 | 0.02 | 0.02 | -4.03 |
| Smoke | Min | 49.71 | 21.64 | 32.29 | 46.32 | 1.30 | 0.17 | 0.10 | -2.27 |

Per load score is the geometric mean of the adjusted desirability:
d_geo=d_((DPF-αT15,100%))=0.1396
With five tested loads, L=5; and α = 0.20, k=⌈0.2×5⌉=1, 〖CVaR〗_0.2 (DPF-αT15,100%) at 20, 40, 60, 80, and 100% loads = 0.2883, 0.4884, 0.5289, 0.3840, 0.1396, respectively. Thus, the worst load is 100% and 〖CVaR〗_0.2 (DPF-αT15) = 0.1396.